

Regular Article

Deposition-based synthesis of nickel-based superalloy microlattices

Dinc Erdeniz ^{a,*}, Tobias A. Schaedler ^b, David C. Dunand ^a^a Department of Materials Science and Engineering, Northwestern University, Evanston, IL 60208, USA^b HRL Laboratories, Malibu, CA 90265, USA

ARTICLE INFO

Article history:

Received 4 May 2017

Received in revised form 17 May 2017

Accepted 17 May 2017

Available online 23 May 2017

Keywords:

Microlattice structures

Micro-architected materials

Ni-based superalloys

Pack cementation

Mechanical behavior

ABSTRACT

Nickel-based superalloy microlattices with periodic hollow struts were fabricated through a combination of two deposition-based methods - electrodeposition and pack cementation - via the following steps: (i) creating a template by self-propagating photopolymer waveguide prototyping, (ii) coating the template with nickel by electroplating, (iii) etching away the template, (iv) coating the Ni lattice with Cr, Al, and Ti by pack cementation, (v) diffusing the Cr, Al, and Ti rich coatings into the nickel to achieve a homogenized alloy and (vi) optionally, aging the alloy to create γ' -precipitates. The resulting nickel-based superalloy microlattices are 2–4 times stronger than pure Ni counterparts.

© 2017 Acta Materialia Inc. Published by Elsevier Ltd. All rights reserved.

Microlattice structures [1–7] are a subgroup of micro-architected materials [8–12] that provide alternatives for stochastic foams. Due to their regular structures, unlike foams, they offer good energy absorption, high specific strength and stiffness, which can be tailored for specific applications by modifying the micro-architecture [13–15]. Microlattices have been fabricated from various metals and alloys using a variety of techniques [16], such as investment casting [17], deformation forming [18], textile techniques [9–11,19], additive manufacturing [5], and the self-propagating photopolymer waveguide technique [2]. In particular, the last method has been used recently to manufacture pure nickel microlattices with a range of relative densities (controlled via wall thickness) resulting in tunable properties [2]. Fabricating such materials from high-temperature alloys, such as Ni-based superalloys, is desirable to create creep- and oxidation-resistant structures that can be actively cooled, using the space between and/or within the hollow struts. Superalloy microlattices are also of interest as cores in lightweight, high-temperature sandwich structures. However, electrodeposition is practically achievable only for pure Ni, and cannot be employed for the complex compositions typical of Ni-based superalloys. One potential solution is to decouple the electro-deposition step, which creates the structure, and a later alloying step. This approach was recently demonstrated for Ni-Cr wires woven into 3D architected structures, to which Al and Ti were added via pack cementation technique, a chemical vapor deposition process, to achieve, after heat treatment, the γ/γ' microstructure and the associated high strength displayed by Ni-based superalloys [9,19–22].

In this study, the pack cementation technique is used to transform pure Ni microlattice structures, fabricated via self-propagating photopolymer waveguide prototyping, into oxidation-resistant and γ' -strengthened Ni-based superalloys. For this purpose, we coat pure Ni microlattices with Cr, Al and Ti via pack cementation, and achieve, after homogenization and aging, a uniform Ni-Cr-Al-Ti composition with γ/γ' superalloy microstructure. We describe here the microstructural evolution during this process and the high-temperature mechanical properties of the resulting structures.

Polymer microlattice templates were fabricated by a self-propagating, photopolymer waveguide process described in detail elsewhere [23]. The polymer structures were then electroplated with ~40 μm nickel using a standard nickel sulfamate plating solution at a low current density of 20 mA/cm². To render the polymer surface electrically conductive for electroplating, a 500 nm nickel layer was deposited by electron beam evaporation using a rotary planetary fixture, achieving complete coverage of the lattice. Electron beam evaporation was selected over electroless nickel deposition to avoid addition of phosphorous, which is detrimental to superalloy properties. After electroplating, the top and bottom surface of the microlattice was sanded to expose the polymer, which was subsequently etched out by immersion in 1.5 M NaOH solution.

For pack chromization, the Ni microlattice was embedded in a pack consisting of 65 wt% alumina (filler), 30 wt% Cr (source), and 5 wt% NH₄Cl (activator) powders contained within an alumina crucible. The loaded crucible was placed at the water-cooled end of a tube furnace flushed with Ar and pushed into the hot zone of the furnace. The deposition process was conducted at 1000 °C for times up to 8 h or until an average of 14 wt% Cr content was achieved, based on weight measurements before and after the treatment. The Cr-rich coatings on the

* Correspondence to: Dinc Erdeniz, 2220 Campus Drive, Cook Hall 2036, Northwestern University, Evanston, IL 60208, USA.

E-mail address: d-erdeniz@northwestern.edu (D. Erdeniz).

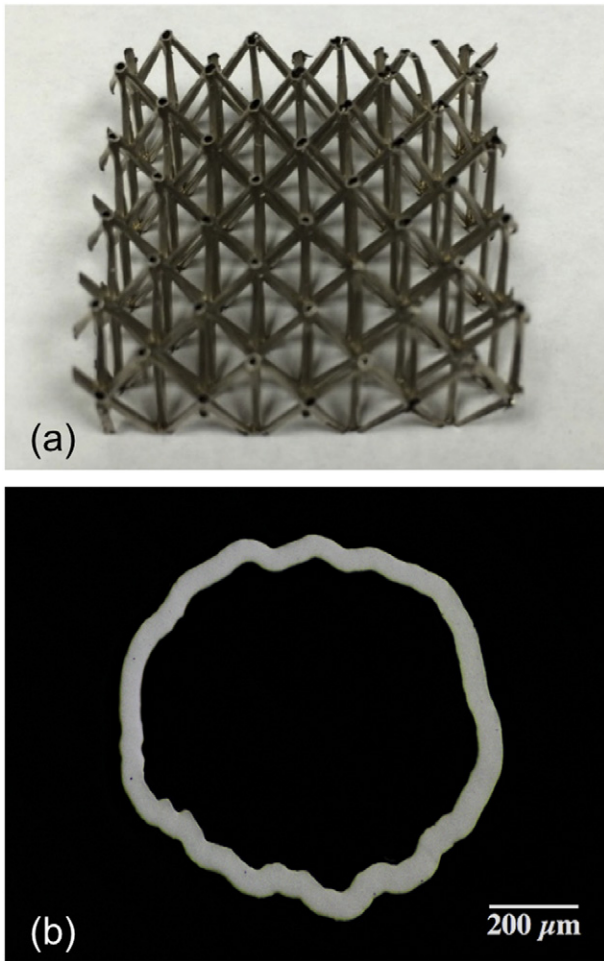


Fig. 1. (a) Photograph of an unalloyed Ni microlattice structure, after electrodeposition and polymer removal, with $35 \times 35 \times 14$ mm dimensions, consisting of $4 \times 4 \times 1$ unit cells (each $\sim 9 \times 9 \times 14$ mm) and (b) optical micrograph of polished radial cross-section of one of the interconnected hollow Ni struts forming the microlattice structure.

inner and outer surfaces of the Ni hollow struts were then diffused into the walls in a homogenization step performed at 1100°C for 24 h under vacuum. Al and Ti were then deposited on the surfaces of the Ni-Cr hollow struts using a similar pack cementation method. The pack consisted of 57 wt% alumina (filler), 30 wt% Ti (source), 10 wt% Raney Ni (Ni-50 wt% Al, source) and 3 wt% NH_4Cl (activator) powders. The sample and the pack were once again placed in an alumina crucible, loaded in the tube furnace at 1000°C and held for 20 min. Aluminotitanized samples were then subjected to a second homogenization treatment ($1100^{\circ}\text{C}/24$ h) to achieve walls with uniform composition, followed by a solutionizing treatment at 1200°C for 2 h and a subsequent aging treatment at 900°C for 16 h, all under vacuum, followed by cooling in the water-chilled furnace. To prevent loss of Al due to evaporation during homogenization and aging, a ~ 10 g piece of Ni-50 wt% Al alloy was placed in the same crucible next to the samples.

Following the heat treatment, the samples were prepared using standard metallographic techniques for optical and scanning electron microscopy (SEM). To reveal γ' precipitates, aged samples were etched for 30 s with a solution consisting of 33 vol% acetic acid, 33 vol% nitric acid, 33 vol% deionized water, and 1 vol% hydrofluoric acid. Compositional data were obtained using an SEM equipped with an energy dispersive X-ray spectrometer (EDS). Hardness data were obtained using a Vickers microhardness tester with an applied load of 10 g and dwell time of 10 s. For each data point, at least five measurements were taken and the average is reported. Hot compression tests were conducted with a strain rate of $5 \times 10^{-4} \text{ s}^{-1}$ at 788°C in air on specimens with

dimensions of 4 unit cells in length (~ 35 mm), 4 unit cells in width (~ 35 mm) and 1 unit cell in height (13–14 mm).

Fig. 1(a) shows a pure Ni microlattice structure prior to alloying, which consists of interconnected hollow struts. A polished cross-section of one of these hollow struts is given in **Fig. 1(b)** that shows the Ni wall with a nearly uniform, $\sim 50 \mu\text{m}$ thickness. The strut does not have a perfectly circular cross-section, which is due to ridges in the surface of the sacrificial polymer scaffold, created via self-propagating photopolymer waveguide prototyping, on the surface of which Ni was deposited. As-deposited Ni has an ultrafine grain structure, hence, a relatively high hardness value of 2.89 GPa (295 HV), which drops to 1.37 GPa (140 HV) upon annealing at 1000°C for 30 min. Grain growth occurred during annealing, as revealed by etched cross-section (not shown here) in which 1–2 grains are typically spanning the entire wall thickness.

The EDS map shown in **Fig. 2(a)** reveals the distribution of Cr in an as-chromized Ni microlattice structure. The image shows a small portion of the radial cross-section of a hollow strut, from a specimen that was chromized at 1000°C for 8 h, which reached an overall Cr content of ~ 14 wt%. The as-coated sample shows high Cr concentration at the outer surface of the strut, as expected, as well as at its inner surface, indicating that the chromium halide gas penetrated into the hollow struts from their open ends, increasing the rate of Cr deposition during pack cementation. The cross-sectional images obtained via optical microscopy (OM) and SEM (in secondary electron mode) revealed little contrast. This indicates that the coating was formed as a solid solution without intermetallic phases, which is not surprising since Ni has a high solubility for Cr (>40 wt% at 1000°C). Upon annealing at 1100°C for 24 h, the

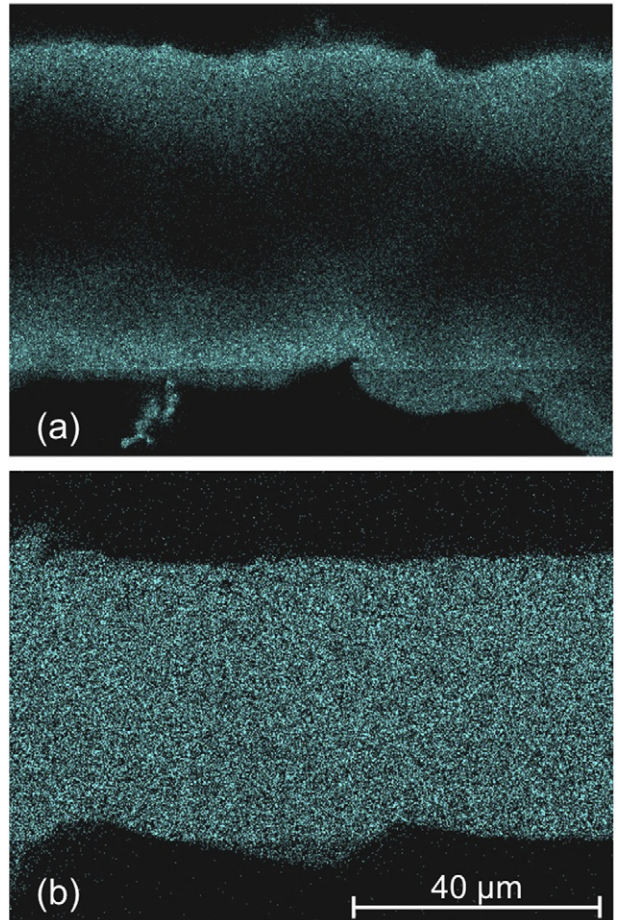


Fig. 2. EDS maps of polished cross-sections, showing the Cr distribution in (a) Cr-coated Ni wall chromized at 1000°C for 8 h showing a Cr gradient from wall surfaces to wall interior and (b) the same sample homogenized at 1100°C for 24 h with a uniform composition of Ni-14 Cr (wt%).

microlattice structure was completely homogenized, achieving a uniform composition, as shown in Fig. 2(b), of Ni-14 wt% Cr. The hardness tests of the homogenized samples show an increased microhardness value of 1.76 GPa (180 HV), compared to 1.37 GPa (140 HV) obtained with the annealed Ni. This increase is expected from the solid solution hardening effect of Cr.

Aluminum and titanium were then simultaneously deposited on the Ni-Cr microlattices via pack cementation, a method previously demonstrated on wires and plates [19,24,25]. Alumino-titanizing at 1000 °C for 15 min resulted in a bilayer coating as shown in Fig. 3(a) and (b). The outer layer was identified, via EDS, as the Ni_2AlTi intermetallic phase and the inner layer was a two-phase mixture of γ' - $\text{Ni}_3(\text{Al,Ti})$ and α -Cr. A similar coating was previously observed in Ref. [19], where Ni-20 wt% Cr wires were alumino-titanized at 1000 °C. This microstructure very likely results from the limited solubility of Cr in the Ni_2AlTi and $\text{Ni}_3(\text{Al,Ti})$ intermetallic layers. Hence, as these coating layers nucleate and grow, Cr is being pushed into the Ni strut until a rejection layer consisting of α -Cr precipitates forms. During the 24 h homogenization treatment at 1100 °C, the α -Cr precipitates dissolve and the solutionized Cr atoms diffuse into the sample. As illustrated in Fig. 3(c), the homogenized microstructure shows a uniform composition of Ni-14Cr-3Ti-1Al (wt%) with no evidence of intermetallics at the strut surfaces. Subsequently, this sample was solutionized at 1200 °C for 2 h and aged at 900 °C for 16 h to form γ' precipitates. The resulting microstructure following the aging treatment is shown in Fig. 3(d), where uniformly distributed, cuboidal γ' precipitates with an average size of 140 nm are present. Higher magnification images (not shown here) also revealed smaller (<10 nm), spherical precipitates within the matrix, expected to be γ' formed during cooling after the aging treatment. The aged sample shows a significant increase in microhardness (3.63 GPa or 370 HV) due to precipitation hardening. Although this value is only 20% higher than for the as-deposited pure Ni (2.89 GPa/295 HV), the precipitation strengthened Ni-14Cr-3Ti-1Al is expected to (i) be creep-resistant at elevated temperatures, (ii) maintain its strength upon long-term exposure

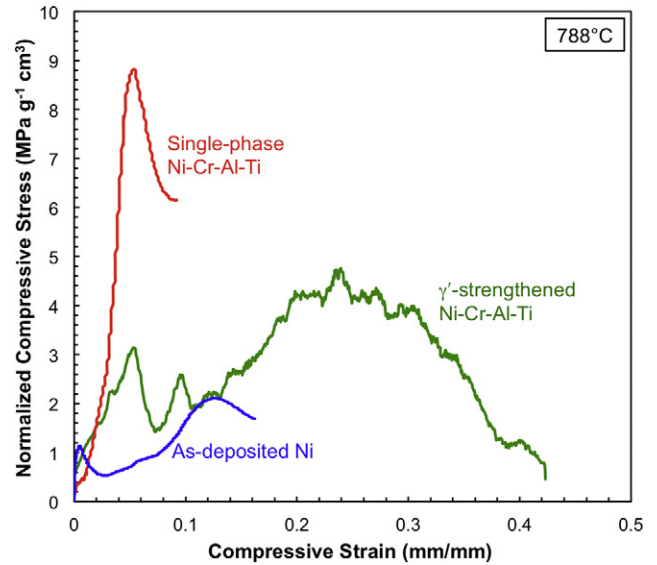


Fig. 4. Normalized stress-strain plots for micro-lattice structures consisting of as-deposited Ni, single-phase Ni-Cr-Al-Ti, and γ' -strengthened Ni-Cr-Al-Ti (in both cases Ni-(10-14)Cr-3Ti-1Al (wt%)), as measured under compression at 788 °C.

at high temperature (i.e., remain coarsening-resistant below the aging temperature of 900 °C) and (iii) show excellent corrosion- and oxidation-resistance due to the presence of Cr and Al. To verify this expectation, hot compression tests were conducted at 788 °C in air.

Fig. 4 shows the normalized stress-strain curves, measured in compression at 788 °C in air, for micro-lattice structures (i) as-deposited Ni, (ii) homogenized, single-phase Ni-(10-14)Cr-3Ti-1Al (wt%), and (iii) aged, γ' -strengthened Ni-(10-14)Cr-3Ti-1Al (wt%). Their relative densities are 1.54, 1.86, and 1.92 %, respectively. As-deposited Ni

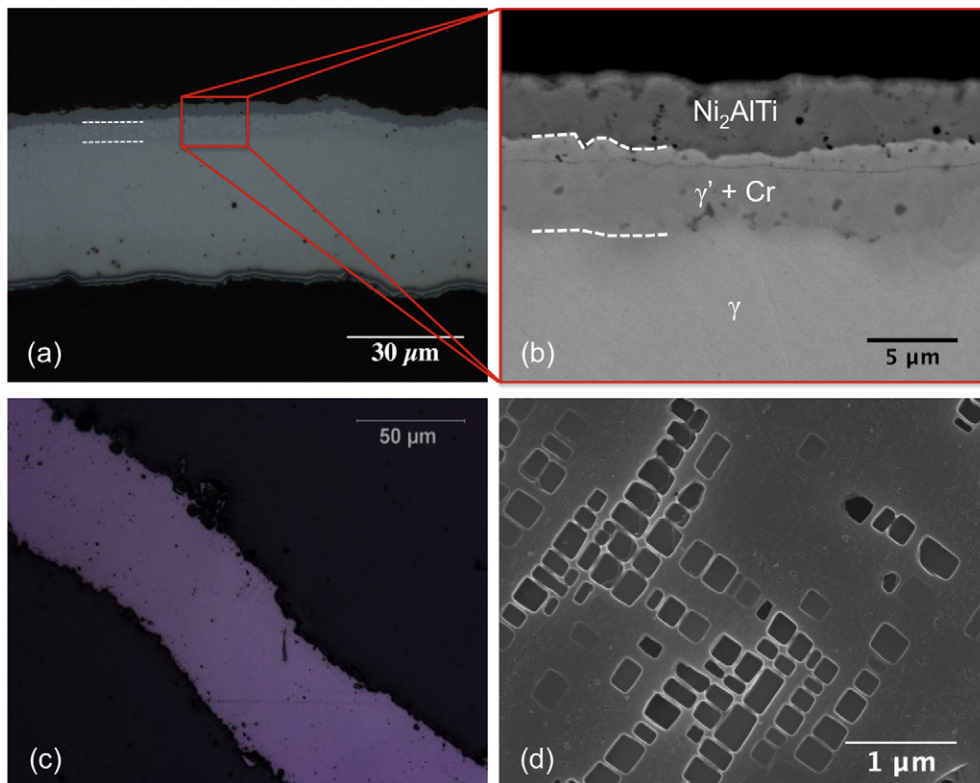


Fig. 3. OM and SEM images showing (a) and (b) Ni-Cr sample as-coated via alumino-titanization at 1000 °C for 20 min showing a two-layer coating marked with dashed lines, (c) the same samples after homogenization at 1100 °C for 24 h exhibiting a uniform composition of Ni-14Cr-3Ti-1Al (wt%), and (d) γ/γ' microstructure achieved after aging at 900 °C for 16 h.

microlattices reached an ultimate strength level of $2.2 \text{ MPa g}^{-1} \text{ cm}^3$ (normalized with density), whereas the single-phase Ni-Cr-Al-Ti samples had an average ultimate strength of $8.1 \text{ MPa g}^{-1} \text{ cm}^3$. This increase is due to solid solution strengthening from Cr, Al, and Ti (along with possible fine γ' -precipitates formed on cooling) along with enhanced oxidation resistance provided by Cr and Al. The aged, γ' -strengthened Ni-Cr-Al-Ti micro-lattice, however, only reached a strength level of $4.8 \text{ MPa g}^{-1} \text{ cm}^3$. These samples showed higher Al concentration closer to both inner and outer surfaces, which resulted in the formation of coarse γ' precipitates that might have reduced the ductility, causing premature failure in these samples. This issue could be resolved by employing a longer homogenization period. Another potential explanation is the sample-to-sample variations in the wall thickness. Since these samples were tested in air, the formation of an oxide layer on the inner and outer surfaces of the hollow struts is expected. The impact of this oxide layer will be more significant for the specimens that have a smaller wall thickness, hence, these samples are more likely to fail via brittle fracture than the specimens with a larger wall thickness.

This study demonstrates a new deposition-based route for the fabrication of thin-walled nickel-base superalloy micro-lattice structures that cannot be processed via other conventional methods. Alloying electrodeposited Ni microlattices with Cr, Al, and Ti significantly improved their high temperature strength, and the process can be optimized to achieve compositions and microstructures with a range of mechanical and physical properties. The methods used here can also be applied to different geometries and scaled up or down to a certain extent. Also, additional elements (e.g., Mn, Fe, Co, Mo) can be added via gas-phase pack cementation [26–28] to further improve the mechanical properties and environmental resistance of the alloy.

The authors acknowledge financial support from the Defense Advanced Research Projects Agency under award numbers W91CRB-10-1-0004 and W91CRB-10-0305 (Dr. Judah Goldwasser, program manager). They also thank Drs. Alan Jacobsen and William Carter (both of HRL) for useful discussions and Sky Park and Angelina Lu (undergraduate students at Northwestern) for their help with sample processing. This work made use of the EPIC facility of Northwestern University's NUANCE Center, which has received support from the Soft and Hybrid Nanotechnology Experimental (SHyNE) Resource (NSF ECCS-1542205); the MRSEC program (NSF DMR-1121262) at the Materials

Research Center; the International Institute for Nanotechnology (IIN); the Keck Foundation; and the State of Illinois, through the IIN, and the MatCI Facility which receives support from the MRSEC Program (NSF DMR-1121262) of the Materials Research Center at Northwestern University.

References

- [1] S. Tsopanos, R.A.W. Mines, S. McKown, Y. Shen, W.J. Cantwell, W. Brooks, C.J. Sutcliffe, J. Manuf. Sci. E. T. ASME 132 (2010).
- [2] T.A. Schaeldler, A.J. Jacobsen, A. Torrents, A.E. Sorensen, J. Lian, J.R. Greer, L. Valdevit, W.B. Carter, Science 334 (2011) 962–965.
- [3] A. Torrents, T.A. Schaeldler, A.J. Jacobsen, W.B. Carter, L. Valdevit, Acta Mater. 60 (2012) 3511–3523.
- [4] Y.L. Liu, T.A. Schaeldler, X. Chen, Mech. Mater. 77 (2014) 1–13.
- [5] P. Li, Z. Wang, N. Petrinic, C.R. Sivior, Mater. Sci. Eng. A 614 (2014) 116–121.
- [6] L. Salari-Sharif, T.A. Schaeldler, L. Valdevit, J. Mater. Res. 29 (2014) 1755–1770.
- [7] J. Xiong, R. Mines, R. Ghosh, A. Vaziri, L. Ma, A. Ohrndorf, H.J. Christ, L.Z. Wu, Adv. Eng. Mater. 17 (2015) 1253–1264.
- [8] N.A. Fleck, V.S. Deshpande, M.F. Ashby, Proc. R. Soc. A 466 (2010) 2495–2516.
- [9] D. Erdeniz, A.J. Levinson, K.W. Sharp, D.J. Rowenhorst, R.W. Fonda, D.C. Dunand, Metall. Mater. Trans. A 46a (2015) 426–438.
- [10] L. Zhao, S. Ha, K.W. Sharp, A.B. Geltmacher, R.W. Fonda, A.H. Kinsey, Y. Zhang, S.M. Ryan, D. Erdeniz, D.C. Dunand, K.J. Hemker, J.K. Guest, T.P. Weihs, Acta Mater. 81 (2014) 326–336.
- [11] J.-H. Lim, K.-J. Kang, Mater. Trans. 47 (2006) 2154–2160.
- [12] Y. Brechet, J.D. Embury, Scr. Mater. 68 (2013) 1–3.
- [13] J.K. Guest, J.H. Prevost, Int. J. Solids Struct. 43 (2006) 7028–7047.
- [14] V.J. Challis, J.K. Guest, J.F. Grotowski, A.P. Roberts, Int. J. Solids Struct. 49 (2012) 3397–3408.
- [15] S.H. Ha, J.K. Guest, Struct. Multidiscip. Optim. 50 (2014) 65–80.
- [16] M.G. Rashed, M. Ashraf, R.A.W. Mines, P.J. Hazell, Mater. Des. 95 (2016) 518–533.
- [17] H.N.G. Wadley, N.A. Fleck, A.G. Evans, Compos. Sci. Technol. 63 (2003) 2331–2343.
- [18] S.J. Johnson, B. Tryon, T.M. Pollock, Acta Mater. 56 (2008) 4577–4584.
- [19] D. Erdeniz, K.W. Sharp, D.C. Dunand, Scr. Mater. 108 (2015) 60–63.
- [20] D. Erdeniz, D.C. Dunand, Intermetallics 50 (2014) 43–53.
- [21] D.C. Dunand, D. Erdeniz, U.S. Patent Office, App. No. 14/592,503 (2015).
- [22] T. Philippe, D. Erdeniz, D.C. Dunand, P.W. Voorhees, Philos. Mag. 95 (2015) 935–947.
- [23] A.J. Jacobsen, W. Barvosa-Carter, S. Nutt, Adv. Mater. 19 (2007) 3892–3896.
- [24] M. Britchi, N. Ene, M. Olteanu, E. Vasile, P. Nita, E. Alexandrescu, Defect Diffus. Forum 297–301 (2010) 1–7.
- [25] F.S. Nogorani, F. Ashrafizadeh, A. Saatchi, Surf. Coat. Technol. 210 (2012) 97–102.
- [26] Q. Pang, Z.Y. Xiu, G.H. Wu, L.T. Jiang, D.L. Sun, Z.L. Hu, J. Mater. Process. Technol. 212 (2012) 2219–2227.
- [27] C. Wang, D.C. Dunand, Metall. Mater. Trans. A 46A (2015) 2249–2254.
- [28] D. Schmidt, M. Galetz, M. Schutze, Oxid. Met. 79 (2013) 589–599.